Material Design & Processing Communications

WILEY

RESEARCH ARTICLE OPEN ACCESS

Influence of Geometry and Size on Precision and Accuracy in Fused Deposition Modeling (FDM) Additive Manufacturing

Nikodmose Moges Gebre | Ilaria Cristofolini | Marco Zago | Pasquale Gallo

Department of Industrial Engineering, Università di Trento, Trento, Italy

Correspondence: Pasquale Gallo (pasquale.gallo@unitn.it)

Received: 14 February 2026 | **Revised:** 3 April 2026 | **Accepted:** 10 April 2026

Academic Editor: Enrico Salvati

Keywords: additive manufacturing | dimensional accuracy | dimensional tolerances | fused deposition modeling | process capability

ABSTRACT

This study presents a systematic evaluation of the dimensional accuracy and process capability of fused deposition modeling (FDM) additive manufacturing, with emphasis on the influence of process-induced thermal and kinematic effects on dimensional performance. Two geometries made of polylactic acid (PLA) were considered: a staircase specimen to assess process capability and directional effects, and a geometric benchmark test artifact (GBTA) to evaluate dimensional reliability across representative features. Measurements were performed using a digital caliper for the staircase model and a coordinate measuring machine (CMM) for the GBTA. Under manufacturer-recommended, unoptimized printing conditions, staircase analysis showed that the investigated FDM system achieved process performance indices (P_m and P_{mk}) ≥ 1.33 at a 95% confidence level. Dimensional stability varied across the build chamber due to spatially nonuniform cooling conditions, with statistically significant position-dependent deviations observed particularly along the build direction. Larger features exhibited higher relative precision. Achievable ISO 286-1 International Tolerance grades ranged from IT9 to IT14. GBTA results confirmed systematic undersizing of cylindrical and curved features. Absolute dimensional deviations remained approximately constant across nominal sizes, whereas percentage errors increased for smaller features due to scale effects. Despite these variations, the geometric form was preserved, demonstrating high repeatability. The proposed capability-based evaluation framework provides a structured approach to quantifying dimensional reliability in polymer-based material extrusion processes for functional components.

1 | Introduction

Additive manufacturing (AM) technologies have evolved from rapid prototyping tools into viable solutions for the batch production of complex functional components. By bypassing the lengthy, multistep sequences inherent to traditional manufacturing routes, AM enables a significant reduction in lead time from initial design to final part delivery, supporting rapid manufacturing strategies across multiple sectors [1–5]. In its broadest definition, AM builds objects layer by layer from three-dimensional CAD models through successive material deposition. Over the past decades, this paradigm has transformed component design and production in a wide range of applications, offering enhanced geometric freedom, reduced tooling requirements, and increased material efficiency.

Compared with conventional manufacturing processes, AM provides substantial advantages in terms of design flexibility, cost-effectiveness for low- to medium-volume production, and the ability to fabricate highly complex geometries with limited postprocessing. Moreover, AM systems are capable of producing multiple assemblies within a single build cycle and can process a broad spectrum of materials, including thermoplastics, composites, metals, and ceramics [6–10]. As a result, AM has found

increasing adoption not only in traditional engineering fields but also in emerging application domains, such as interior design and consumer products [11].

In parallel with industrial adoption, the increasing availability of high-performance desktop FDM systems has enabled distributed manufacturing scenarios, where functional components can be locally produced, replaced, or customized by end users. This transition supports circular economy strategies by facilitating repair, personalization, and life-extension of consumer products through on-demand fabrication [12, 13]. In these distributed contexts, dimensional reliability remains essential to ensure functional compatibility and esthetic quality, even when components are produced under nonoptimized, user-level conditions.

Dimensional tolerances (DTs) therefore play a critical role in ensuring functional compatibility, assembly accuracy, and overall product quality [14]. Similar to other manufacturing technologies, DT defines the permissible limits of variation in a part's physical dimensions and is essential for meeting functional, mechanical, and assembly requirements. However, the intrinsic characteristics of AM processes, including layer-by-layer material deposition, thermal gradients, material shrinkage, surface roughness, and process-induced anisotropies, introduce sources of dimensional variability that are often more pronounced than in conventional manufacturing [15, 16].

Among the various AM technologies, fused deposition modeling (FDM) is one of the most widely adopted material extrusion processes. In FDM, a semimolten thermoplastic filament is extruded through a heated nozzle and deposited layer by layer, where it cools and solidifies to form a consolidated structure. Interlayer bonding is governed primarily by thermal energy and material diffusion at the interface between adjacent filaments. Owing to its relatively low cost, operational simplicity, and compatibility with widely available materials such as polylactic acid (PLA), acrylonitrile butadiene styrene (ABS), and elastomers, FDM is extensively used for both prototyping and functional part production [17, 18]. Nevertheless, FDM typically exhibits lower dimensional accuracy and surface quality compared with conventional manufacturing processes, largely due to the staircase effect, thermally induced deformations, and the need for auxiliary support structures [19, 20]. To mitigate these limitations, alternative support strategies and postprocessing approaches have been proposed, including adaptive build platforms and surface finishing techniques aimed at reducing distortion and improving dimensional stability [4, 21]. In parallel, several studies have shown that key printing parameters such as layer strategy and deposition orientation strongly influence mechanical performance and structural response, particularly in high-performance polymers [2]. Early experimental studies in dimensional precision and accuracy analysis showed deviations along the X, Y, and Z directions, demonstrating that dimensional accuracy is direction- and size-dependent and nonuniform across the build volume [22]. Subsequent investigations confirmed the significant, geometry-dependent influence of process parameters such as layer thickness, orientation, building temperature, part geometry, and build direction [15, 23]. More recent contributions attempted to benchmark FDM dimensional performance against conventional manufacturing by referencing ISO tolerance grades, reporting the achievable tolerance range [24].

Although shrinkage and spatial nonuniformity in FDM are well documented, most existing studies are conducted under optimized or laboratory-controlled parameter settings and focus on isolated geometric features or specific components. Systematic statistical validation of process capability across spatial build regions remains limited, and dimensional performance is rarely framed within standardized tolerance systems or linked to representative functional geometries. Consequently, the assessment of FDM accuracy using process capability concepts and international tolerance standards is still insufficiently developed [25, 26].

With the growing adoption of AM across sectors such as furniture, aerospace, biomedical, and automotive applications, a systematic and transferable evaluation of dimensional accuracy and precision has become increasingly important. This need is particularly relevant in distributed manufacturing contexts, where consumer-level systems are used to fabricate replacement or customized components without extensive parameter optimization. In such scenarios, quantifying achievable tolerance grades under manufacturer-recommended, unoptimized settings becomes critical to assess functional interchangeability.

In this context, the present study addresses this gap by evaluating the dimensional performance of FDM as a manufacturing process rather than as a collection of isolated part measurements, focusing specifically on machine-related dimensional reliability under manufacturer-recommended, unoptimized conditions representative of consumer-level operation. An experimental framework is proposed that combines geometry-dependent benchmarking with process capability analysis and standardized tolerance classification. Two complementary test geometries are employed. First, a staircase specimen is designed to systematically cover ISO 286-1 dimensional size ranges along the printer's X, Y, and Z axes, enabling an objective assessment of machine accuracy and precision independent of the final component geometry. Second, a geometric benchmark test artifact (GBTA) is used to evaluate dimensional reliability in the context of a real-world application. As a case study, the GBTA is specifically designed to capture the geometric complexity characteristic of the door-handle component developed and presented in [11]. The artifact and its feature groups are described in detail in Section 2.2.2.

The contribution of this work, therefore, lies in the integration of capability-based statistical validation, ISO 286-1 tolerance classification, and geometry-representative benchmarking under realistic consumer-level FDM operating conditions. The paper is organized as follows: Section 2 describes the experimental framework and methodologies. Section 3 presents and discusses the results, and Section 4 summarizes the main findings.

2 | Materials and Methods

Figure 1 illustrates the workflow for evaluating DT in the FDM process. Using a Bambu Lab X1-Carbon FDM printer and PLA filament, two distinct geometries were produced: staircase parts

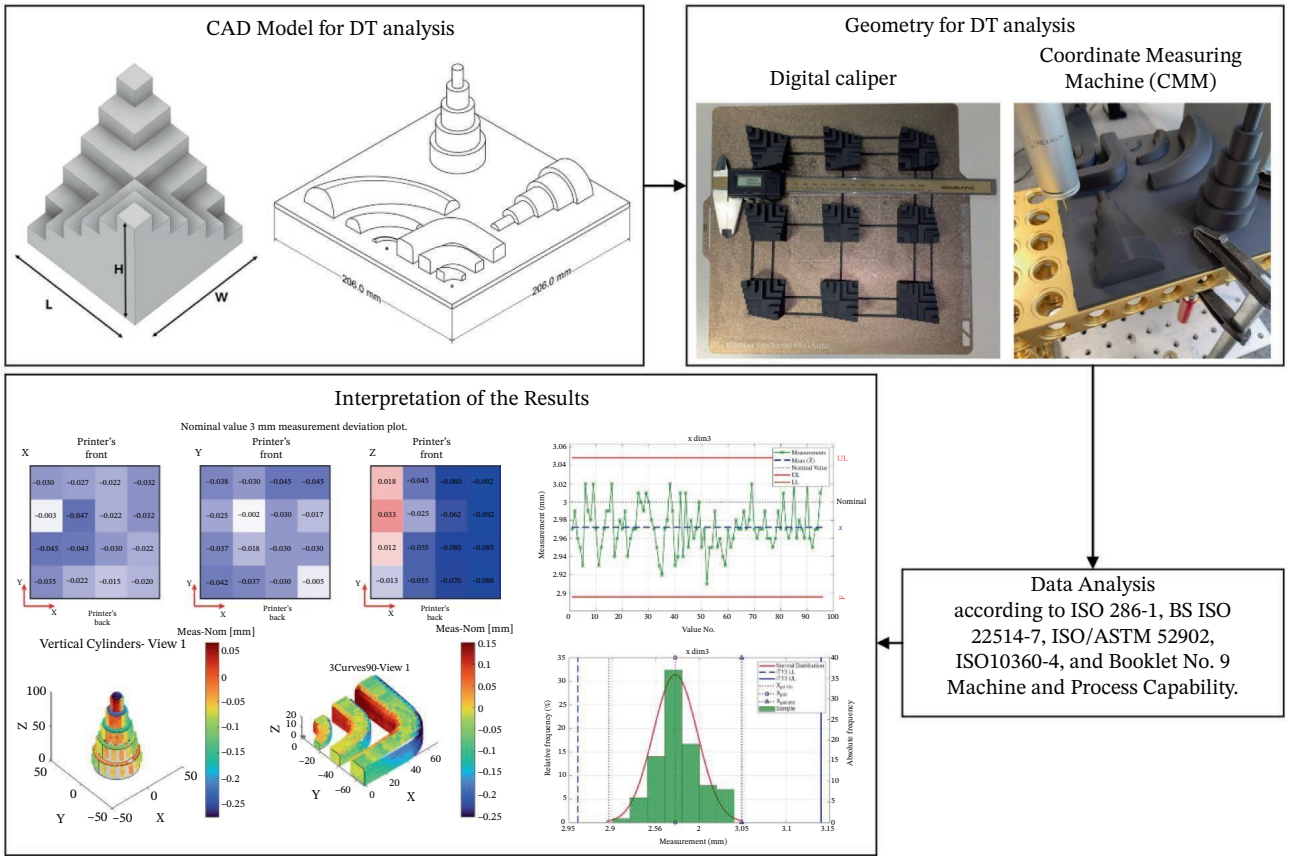

FIGURE 1 | Dimensional tolerance (DT) measurement workflow integrating test model design, dimensional measurement, and data analysis.

TABLE 1 | Mechanical and physical properties of the commercial PLA filament [29, 30].

Material	E(GPa)	γ	Yield strength (MPa)	UTS (MPa)	Density (g/cm^3)	Elongation (%)
PLA	3.5	0.36	70	73	1.25	7

for systematic measurements across the build platform and a GBTA part to assess multifeature door-handle dimensions. Following fabrication, samples were measured using a digital caliper and a coordinate measuring machine (CMM). The resulting data were analyzed according to ISO and ASTM standards to assess printer accuracy and precision.

2.1 | Materials

PLA filament was used to fabricate test specimens. PLA was selected due to its widespread availability, ease of processing, relatively low warping tendency, and common use in consumer-level FDM applications, particularly for nonstructural interior components. PLA has the following thermal properties: glass transition temperature (55°C–65°C), melting temperature (150°C–155°C), and degradation temperature (300°C–370°C) [27, 28]. Table 1 summarizes the mechanical and physical properties provided by the supplier (Bambu Lab Co.).

The specimens were fabricated using a Bambu Lab X1-Carbon FDM printer equipped with a 0.4 mm nozzle and a 1.75 mm filament diameter. The selected printer represents a commercially available high-performance desktop system. Printing parameters correspond to manufacturer-recommended settings and were intentionally not optimized, in order to evaluate dimensional performance under baseline consumer-level operating conditions. Printing parameters included a layer height of 0.16 mm; 100% infill with a ±45 linear pattern for staircase specimens (Figure 2); and 15% infill with a gyroid pattern for GBTA specimens (see Section 2.2.2). Full infill was adopted for staircase samples to minimize internal structural variability and isolate machine-related dimensional effects. In contrast, a 15% infill was selected for the GBTA to reflect realistic production conditions for the component taken as an example [11], where reduced material usage and printing time are typical. Although infill percentage can influence global thermal mass and shrinkage behavior, dimensional deviations in FDM are primarily governed by contour deposition and external boundary cooling, which remain comparable between configurations.

The chamber and build plate temperatures were set to 37°C and 55°C, respectively, with a constant nozzle temperature of 220°C. The build volume of the printer is 256 × 256 × 256 mm.

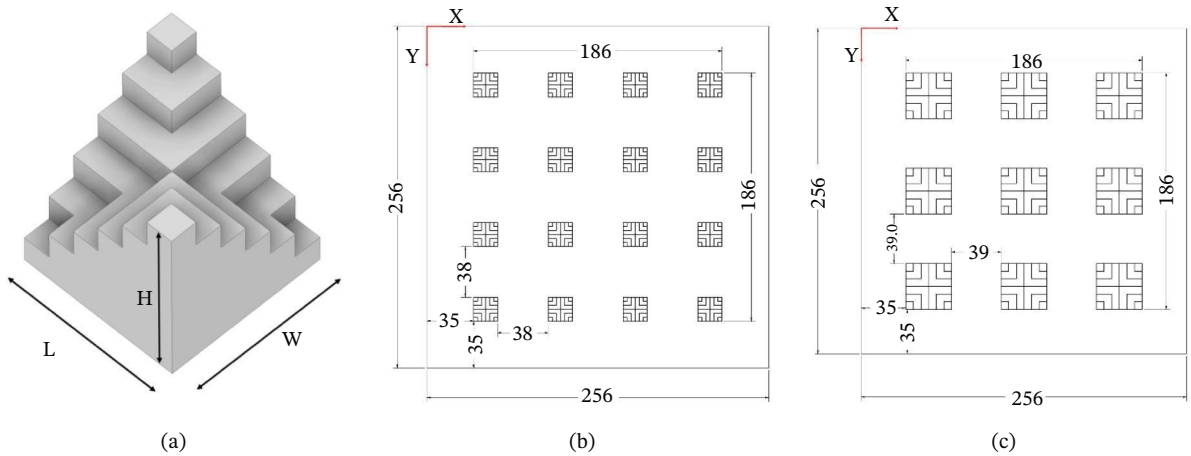

FIGURE 2 | Benchmark staircase geometries used for dimensional tolerance measurements: (a) single staircase part, (b) Geometry 1 featuring a distribution of 4×4 benchmark staircase with $L = W = H = 18$ mm, and (c) Geometry 2 featuring a 3×3 benchmark staircase distribution with $L = W = H = 36$ mm. All dimensions are in mm. Detailed dimensions of the staircase part are provided in Appendix A.

2.2 | Dimensional Tolerances (DT)

2.2.1 | DT Sample

The COMPAQT (component for machine performance assessment in quick time) reference geometry [24] was modified to fit the build volume of the Bambu Lab X1-Carbon printer and to accommodate multiple DT measurement ranges. The CAD models were created using Autodesk Inventor Professional 2025, and STL files were exported for slicing.

Figures 2 and 3 illustrate the modified staircase geometries and their layout on the build platform (CAD models and real samples, respectively). The staircase parts have nominal dimensions of $18 \times 18 \times 18$ and $36 \times 36 \times 18$ mm. Figure 2a shows a single staircase geometry used for DT measurements, whereas Figure 2b,c depict the distribution of staircase parts across the build platform.

To extend the measurable size range beyond a single part, multipart builds were conducted using 16 and 9 staircase specimens distributed across the build platform. This configuration extended the measurable range to 186 mm along the X and Y axes, whereas the Z-axis measurements remained limited by the part height. In total, more than 2076 measurements were collected for the X and Y axes and 900 measurements for the Z axis.

2.2.2 | Geometric Benchmark Test Artifact (GBTA)

Figure 4 presents the GBTA developed to assess dimensional accuracy and geometric fidelity for door-handle manufacturing (see [11]). Door-handles exhibit a wide range of shapes and sizes governed by both functional and ergonomic requirements. The idea behind the geometry is to cover different shapes and complex features required for such components. Therefore, the GBTA shows and gives priority to curved surfaces, diameter changes, and shape transitions. Some geometrical features are therefore excluded (e.g., unsupported overhangs, holes). Nevertheless, the methodological framework can be extended to those features and/or other GBTA.

FIGURE 3 | FDM-printed modified COMPAQT staircase parts on the build plate: (a) $18 \times 18 \times 18$ mm^3 arranged in a 4×4 grid layout, and (b) $36 \times 36 \times 36$ mm^3 arranged in a 3×3 grid layout.

2.2.3 | DT Measurement

Dimensional measurements were performed using a digital caliper (Mitutoyo Corporation, Japan) for staircase samples and a CMM (Hexagon, Sweden) for GBTA specimens (equipped with a 1 mm sphere tip working in point acquisition mode), due to the different complexity of the different features. Measurements were conducted at room temperature directly on the build platform, as shown in Figure 5.

The digital caliper has a resolution of 0.01 mm and a manufacturer-declared accuracy of ± 0.02 mm. This measurement uncertainty is at least one order of magnitude smaller than the evaluated tolerance intervals (typically ≥ 0.1 mm for the investigated nominal ranges) and is therefore adequate for assessing process capability of the staircase geometries. The CMM was adopted for the GBTA due to the presence of curved and orientation-dependent features requiring higher geometric fidelity. The maximum permissible error (MPE) of the CMM system is $(2.2 + L/300)\,\mu$m, in accordance with ISO 10360-4. This ensures measurement uncertainty significantly lower than the observed dimensional deviations.

2.2.3.1 | Staircase Sample (Modified COMPAQT). The evaluation of attainable precision and accuracy in FDM involves two main steps: collection of dimensional measurements and post-processing of the data according to international standards and relevant literature [24, 31–37].

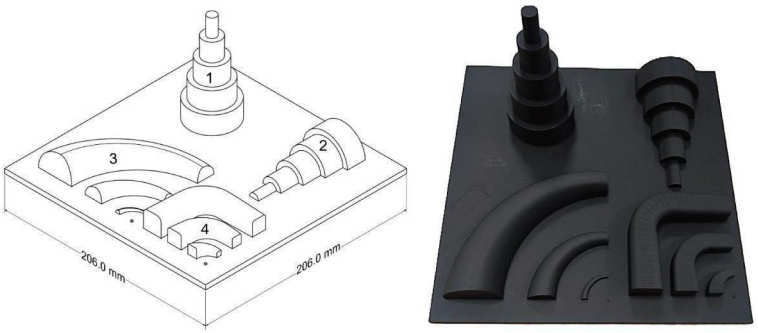

FIGURE 4 | Geometric benchmark test artifact (GBTA) designed for door-handle manufacturing applications. The artifact incorporates four feature groups: vertical cylinders (1), horizontal cylinders (2), 3-curved profiles (3), and 3-curved 90° features (4).

(a) (b)

FIGURE 5 | Measurement setup for dimensional tolerance evaluation of (a) the staircase parts using a digital caliper and (b) the geometric benchmark test artifact (GBTA) using a coordinate measuring machine (CMM).

1. Data grouping: Measurements were grouped according to build direction (X, Y, and Z), nominal dimension (3 mm, 6 mm, etc.), and spatial location on the build plate. The selected nominal dimensions are reported in Appendix B, which reports the standard ISO 286-1 tolerance grades for nominal sizes up to 250 mm. In addition to that, the build platform was subdivided into two regions based on relative position with respect to the cooling fan (fan-side vs. opposite-side), enabling quantitative comparison of location-dependent deviations using a t-test analysis as reported in Appendix C.

2. Deviation calculation: The deviation D_i between the nominal size N_i and the measured value M_i was calculated as:

$$D_i = M_i - N_i \tag{1}$$

3. Distribution fitting: Measurement distributions were analyzed following ISO 22514 recommendations. The measurement data were first fitted using normal, log-normal, folded-normal, gamma, Rayleigh, and Weibull distributions. Subsequently, the best-fitting distribution was selected using the Kolmogorov–Smirnov goodness-of-fit test at a 95% confidence level, based on the highest p value associated with the distribution fit. Percentile-based descriptors were adopted to avoid strict normality assumptions and to ensure robustness of capability estimation.

4. Performance indices calculation: Machine performance was quantified using the potential (P_m) and actual (P_{mk}) performance indices. Lower (LL) and upper (UL) specification limits were derived from ISO 286-1 tolerance grades.

The index P_m reflects the potential precision of the process under ideal centering, whereas P_{mk} represents the actual manufacturing capability and is directly related to the expected proportion of out-of-specification parts. From a manufacturing perspective, P_{mk} is the most relevant indicator, as it directly relates to the proportion of parts expected to fall outside specification limits.

Percentiles extracted from the fitted distributions and used to compute:

$$P_i = \frac{UL - LL}{X_{99.865\%} - X_{0.135\%}} \tag{2}$$

$$P_{MK} = \min\left(\frac{X_{50\%} - LL}{X_{50\%} - X_{0.135\%}}, \frac{UL - X_{50\%}}{X_{99.865\%} - X_{50\%}}\right) \tag{3}$$

5. Specification limits for target capability: A target capability threshold of $P_{mk} = 1.33$ was selected, corresponding to a widely adopted minimum industrial benchmark for stable manufacturing processes. Under this criterion, the tolerance interval is defined according to the selected distribution curve:

$$\mathrm{UL} - \mathrm{LL} = 1.33 \times \left(X_{99.865\%} - X_{0.135\%}\right) \tag{4}$$

$$\mathrm{LL} = X_{50\%} - 1.33 \times \left(X_{50\%} - X_{0.135\%}\right), \mathrm{UL} = X_{50\%} + 1.33 \times \left(X_{99.865\%} - X_{50\%}\right) \tag{5}$$

This threshold corresponds to approximately 66 parts per million outside specification under normal distribution assumptions (Table 2). Higher capability levels (e.g., $P_{mk} \geq 1.67$), typically associated with highly optimized industrial processes and applications such as aerospace and electrical components, were considered outside the scope of the present baseline study. Table 2 summarizes the estimated proportion of out-of-specification parts under the assumption of normally distributed data, expressed as a function of the process capability index P_{mk} [38].

6. Uncertainty evaluation: Because $P_m$and $P_{mk}$are estimated from finite samples, 95% confidence intervals were computed using the χ^2 distribution:

$$P_{m,\min} = \sqrt{\frac{\chi^2_{n-1,\alpha/2}}{n-1}} P_m \tag{6}$$

$$P_{m,\max} = \sqrt{\frac{\chi^2_{n-1,1-\alpha/2}}{n-1}} P_m \tag{7}$$

$$P_{mk,\min} = \sqrt{\frac{\chi^2_{n-1,\alpha/2}}{n-1}} P_{mk} \tag{8}$$

$$P_{mk,\max} = \sqrt{\frac{\chi^2_{n-1,1-\alpha/2}}{n-1}} P_{mk} \tag{9}$$

TABLE 2 | Estimated proportion of out-of-specification parts (ppm) as a function of the process capability index P_{mk}, including the distance between the upper (UL) and lower (LL) specification limits, and the typical application areas [36, 38].

P_{mk}	Out-of-specification parts (ppm)	UL − LL distance	Note
1.00	2600	6σ	Standard/commodity components
1.33	66	8σ	General engineering components
1.67	0.54	10σ	Safety-critical components
2.00	0.002	12σ	Electrical/highly critical components

In addition to capability evaluation, spatial deviations between two build regions, that is, the fan-side and the opposite-side, were studied. To this aim, a two-sample t-test (Appendix C) at a 95% confidence level ($\alpha = 0.05$) was conducted to determine whether the proximity to the cooling fan introduces statistically significant differences in the dimensional accuracy of the printed staircase parts.

2.2.3.2 | GBTA Sample. A hierarchical datum reference system was defined for each feature group. The plane containing all features was used as the primary datum (Datum A), followed by secondary (Datum B) and tertiary (Datum C) datums selected according to the geometry under inspection. For vertical and horizontal cylinders, Datum B was defined by a reference plane parallel to the build plate and Datum C by the cylinder axis. For the 3-curves 90° feature, Datum B and Datum C were defined by planes parallel to the XZ and YZ planes, respectively. Figure 6 illustrates the measurement setup and datum definition.

3 | Results and Discussion

The following discussion interprets the experimental results in terms of the underlying FDM process mechanisms, with particular emphasis on the role of thermal gradients, deposition kinematics, and geometric scale in determining dimensional accuracy and process capability.

3.1 | Staircase Samples

Measurements of the staircase parts were conducted at 16 spatial locations for Geometry 1 and 9 locations for Geometry 2 (see Figure 2), yielding over 240-dimensional distributions. Representative process control charts and dimensional distributions for the X, Y, and Z directions are shown in Figure 7. Histograms (left) show measured-dimension distributions overlaid with fitted normal distributions, whereas control charts (right) display measurement sequences with 3σ limits and ISO tolerance limits.

The results indicate that the dimensional data closely follow normal distributions, with most measurements centered near the nominal values. The overall mean deviations (measured minus nominal) were -0.02 ± 0.04 mm in the X direction, -0.03 ± 0.04 mm in the Y direction, and -0.03 ± 0.05 mm in the Z direction. The 3σ limits fall well within the IT13 tolerance limits for the representative cases shown, confirming stable process behavior. Slight negative mean deviations were observed for most single-part measurements, whereas multipart

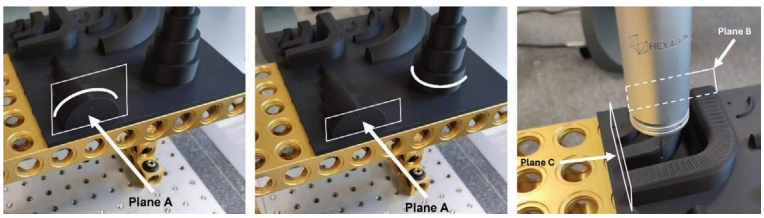

FIGURE 6 | CMM measurement setup and hierarchical datum reference system for the GBTA feature groups. The picture shows the datum plane and the feature being measured (white curved lines).

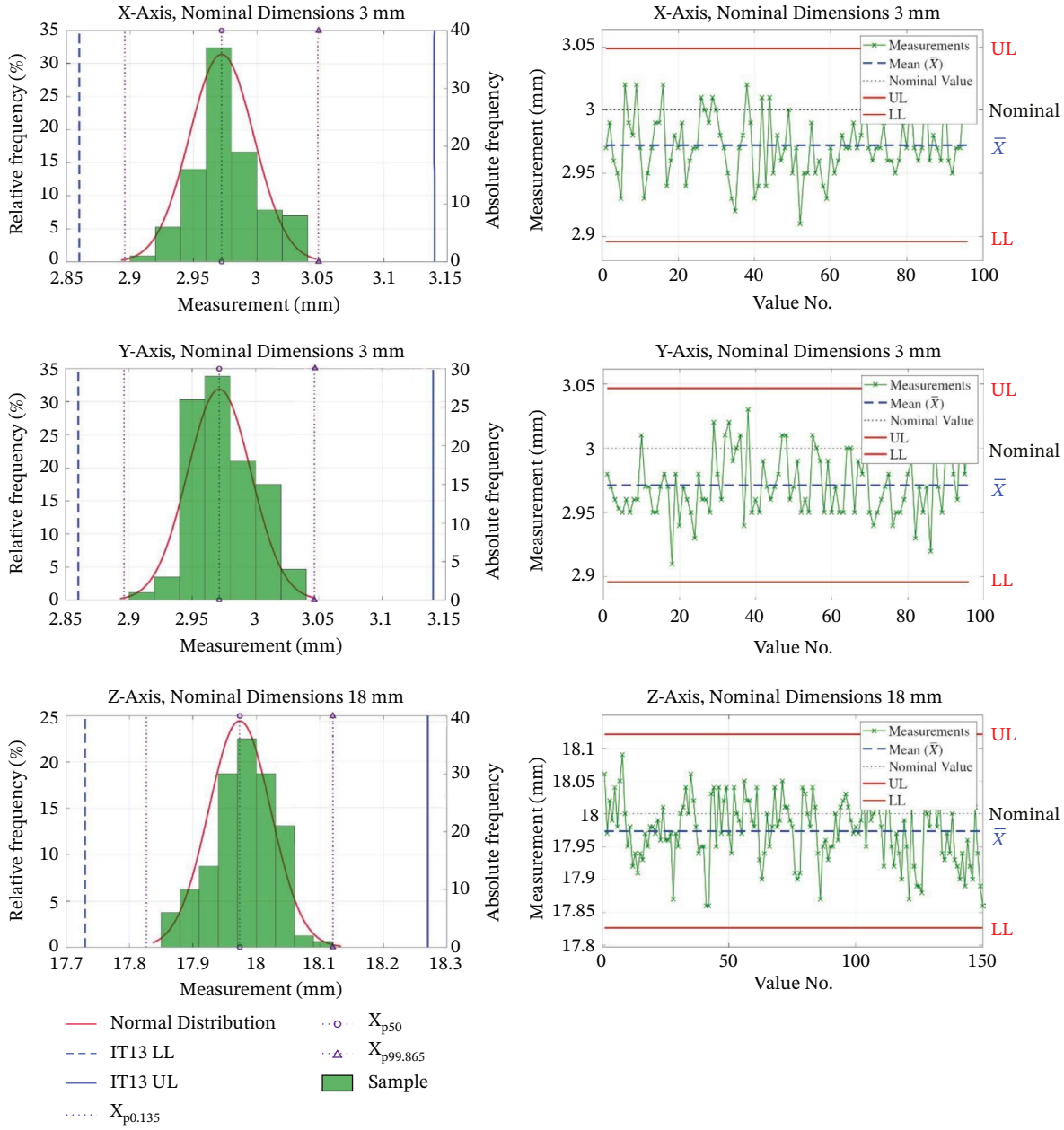

FIGURE 7 | Process control charts and dimensional distributions for representative X (3 mm), Y (3 mm), and Z (18 mm) measurements. Left: histograms with fitted normal distributions. Right: control charts showing 3σ limits and ISO tolerance limits. Note: The equations to calculate the mean, standard deviation, LL (lower limit), and UL (upper limit) are reported in Section 2.2.3.

measurements occasionally exhibited small positive shifts due to cumulative thermal effects during printing.

Figures 8 and 9 show, as an example, a few selected heat maps of average deviations for Geometry 1 and Geometry 2 staircase parts, respectively. The complete heat map dataset is available in Appendix D instead. The color maps reveal spatially dependent deviations across the build plate. For Geometry 1, negative deviations dominate along the Z direction on the side of the build plate adjacent to the cooling fan, whereas positive deviations are observed on the opposite side, indicating nonuniform cooling. The reduced dimensional precision observed along the Z direction can be attributed to the layer-wise nature of material extrusion, where discretization effects and cumulative thermal contraction act normal to the build plane. Similar spatial cooling gradients and direction-dependent shrinkage behavior have been reported in previous FDM dimensional investigations [39–42]. In contrast, in-plane dimensions (X and Y) benefit from continuous filament deposition and stronger geometric constraints during solidification.

Geometry 2 exhibits scale-dependent behavior, with larger nominal dimensions showing increased shrinkage and smaller dimensions exhibiting slight expansion. This size-dependent behavior reflects differences in thermal mass and cooling kinetics: larger features experience more uniform cooling and stress redistribution, whereas smaller features are more sensitive to localized heat dissipation, resulting in higher relative dimensional deviations [43–45].

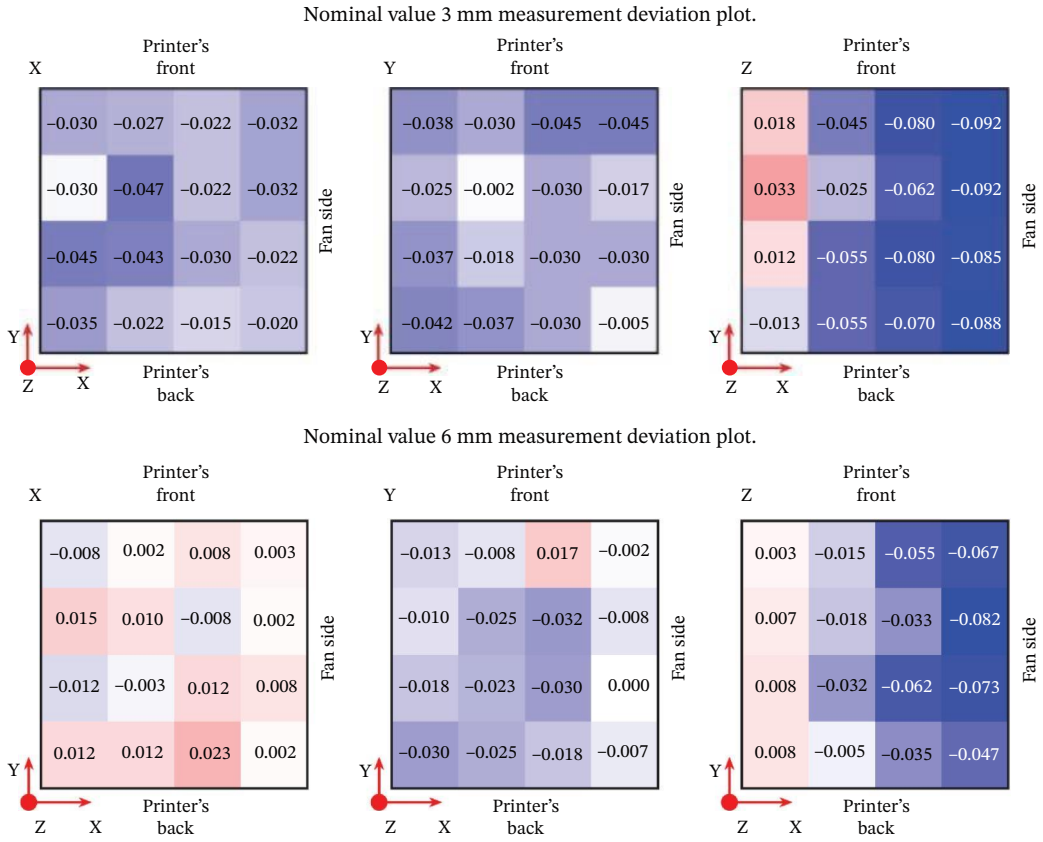

FIGURE 8 | Selected heat maps of average relative deviations (mm) for Geometry 1 staircase parts at nominal dimensions of 3 and 6 mm. Each square represents a measurement location within the build chamber. Blue indicates negative deviations (shrinkage), whereas red indicates positive deviations (expansion). The complete dataset is provided in Appendix D.

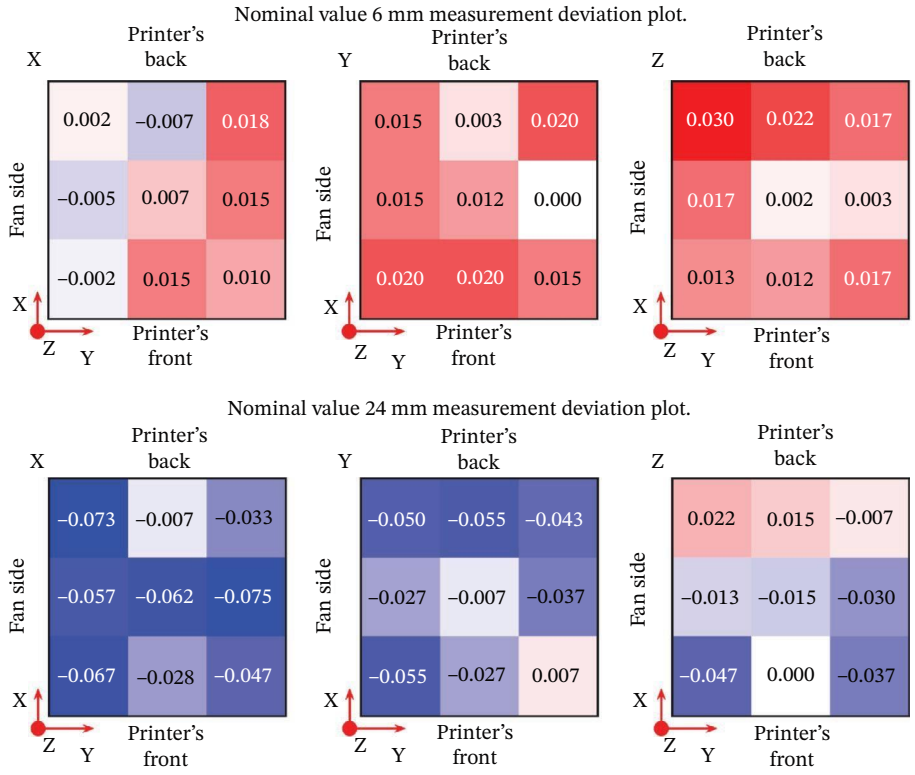

FIGURE 9 | Selected heatmaps of average relative deviations (mm) for Geometry 1 staircase parts at nominal dimensions of 6 and 24 mm. Each square represents a measurement location within the build chamber. Blue indicates negative deviations (shrinkage), whereas red indicates positive deviations (expansion). The complete dataset is provided in Appendix D.

To quantitatively assess the spatial deviation patterns observed in Figures 8 and 9, mean deviations for each measurement location were compared between fan-side and opposite-side regions using a two-sample t-test ($\alpha = 0.05$) for both Geometry 1 and Geometry 2. Details of the statistical procedure are reported in Appendix C. For Geometry 1, the Z direction exhibited a statistically significant difference ($p < 0.001$), whereas comparisons for the X and Y directions resulted in nonsignificant p values of 0.984 and 0.132, respectively. These results indicate that no statistically significant difference was observed between fan-side and opposite-side regions in the X and Y directions, suggesting that in-plane dimensional accuracy is not strongly affected by build plate position. In contrast, the Z direction shows higher negative deviations on the fan-side. This behavior is consistent with localized cooling effects or thermal gradients influencing layer height consistency, indicating that the observed Z-axis deviations are governed by systematic process phenomena rather than random variability. In the case of Geometry 2, the Z direction yielded a nonsignificant p value of 0.77. Corresponding comparisons for the X and Y directions yielded p values of 0.405 and 0.822, respectively. Unlike Geometry 1, these results indicate no statistically significant difference in dimensional accuracy between fan-side and opposite-side regions for Geometry 2. This suggests that the spatial deviation patterns are less pronounced for larger geometries. A possible explanation is that larger parts require longer layer deposition times, allowing more uniform thermal dissipation and reducing the influence of localized cooling gradients. This interpretation is consistent with the more homogeneous deviation patterns observed in the heat maps (Figures 8, 9, A4 and A5). For clarity, global mean deviations refer to aggregated measurements across all locations, whereas the t-test analysis is performed using mean deviations computed for each measurement location.

Figure 10 summarizes the achievable tolerance interval capabilities as a function of nominal size according to ISO 286-1, computed using Equations (4) and (5). A process capability of $P_{mk} \geq 1.33$ was achieved for all evaluated sizes with 95% confidence, indicating stable and consistent dimensional performance across the investigated build configurations. Expressing FDM dimensional performance in terms of ISO 286-1 tolerance grades provides a manufacturing-oriented interpretation of process capability, enabling direct comparison with conventional production processes [45–47] and facilitating the integration of additively manufactured components into tolerance-driven design workflows.

Table 3 summarizes the achievable ISO 286-1 IT grades for staircase parts fabricated using the Bambu Lab X1-Carbon FDM printer. The results are reported at a 95% confidence level with P_m and $P_{mk} \geq 1.33$ and include the lower limit (LL), midpoint (M), and upper limit (UL) of each tolerance interval.

Table 4 summarizes the achievable ISO 286-1 IT grades for staircase parts considered in the present work, compared with conventional manufacturing processes. The results indicate that FDM parts in this study achieved IT grades primarily between IT9 and IT14, depending on the measurement axis. In comparison, traditional processes such as CNC turning and milling reach higher precision (lower IT grades, IT7-IT10), whereas injection molding typically achieves IT8-IT12. Other processes, such as casting and sintering, show wider tolerance ranges (IT10-IT16), highlighting the advantage of FDM over some conventional methods but also its limitations compared with high-precision machining. This finding is particularly relevant for applications such as nonstructural components or functional prototypes, where FDM may offer sufficient dimensional performance for functional compatibility and acceptable esthetic quality, without necessarily requiring the ultratight tolerances of high-end machining.

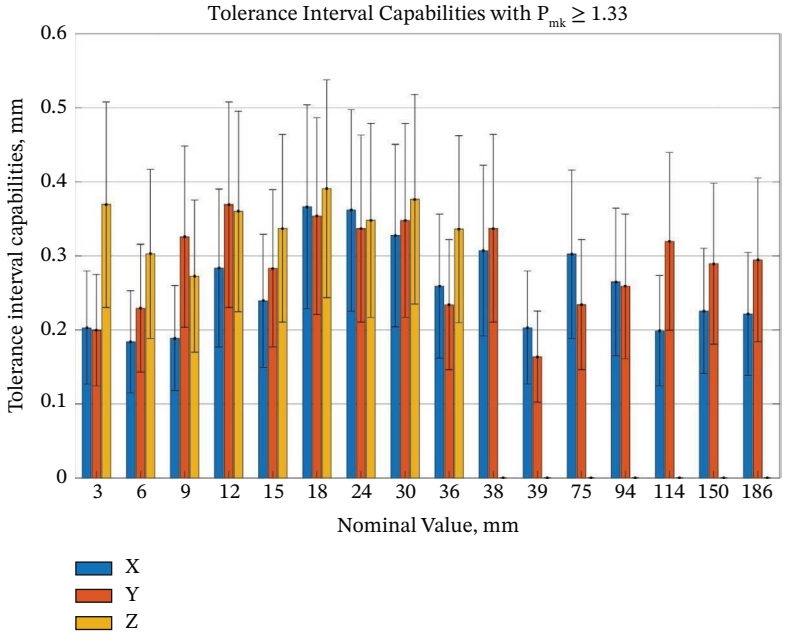

FIGURE 10 | Achievable tolerance interval capabilities as a function of nominal size for the staircase samples, evaluated along the X, Y, and Z axes with a minimum process capability threshold of $P_{mk} \geq 1.33$ as defined by ISO 286-1. Error bars represent the associated uncertainty of each tolerance interval estimate.

TABLE 3 | Achievable IT grades according to ISO 286-1 for staircase parts fabricated on the Bambu Lab X1-Carbon FDM printer. Values are based on a 95% confidence level with P_m and $P_{mk} \geq 1.33$ including the lower limit (LL), midpoint (M), and upper limit (UL) of each interval.

Size, mm	ISO 286-1 range, mm		IT grade			*X*, mm			*Y*, mm			*Z*, mm		
Size	Above	Up to	*X*	*Y*	*Z*	LL	M	UL	LL	M	UL	LL	M	UL
3	1	3	13	13	14	2.90	2.97	3.05	2.90	2.97	3.05	2.81	2.95	3.09
6	3	6	12	12	13	5.94	6.01	6.07	5.91	6.00	6.08	5.87	5.99	6.10
9	6	10	11	13	13	8.93	9.00	9.07	8.85	8.98	9.10	8.85	8.95	9.06
12	6	10	12	13	13	11.87	11.97	12.08	11.83	11.97	12.11	11.84	11.98	12.11
15	10	18	12	13	13	14.86	14.95	15.04	14.82	14.93	15.03	14.81	14.94	15.07
18	10	18	13	13	13	17.83	17.97	18.10	17.84	17.97	18.10	17.83	17.97	18.12
24	18	30	13	12	12	23.81	23.95	24.09	23.84	23.97	24.09	23.86	23.99	24.12
30	18	30	12	12	12	29.83	29.96	30.08	29.84	29.97	30.10	29.84	29.98	30.13
36	30	50	11	11	11	35.86	35.96	36.06	35.87	35.96	36.05	35.86	35.98	36.11
38	30	50	11	11		37.89	38.00	38.12	37.89	38.02	38.14			
39	30	50	10	10		38.96	39.04	39.11	38.96	39.02	39.08			
75	50	80	11	10		74.86	74.97	75.09	74.88	74.96	75.05			
94	80	120	10	10		93.89	93.99	94.09	93.90	94.00	94.10			
114	80	120	9	10		113.91	113.98	114.06	113.87	113.99	114.11			
150	120	180	9	10		149.89	149.98	150.06	149.88	149.99	150.10			
186	180	250	9	9		185.91	185.99	186.07	185.88	185.99	186.10			

TABLE 4 | Comparison of the ISO 286-1 IT grade for various manufacturing processes [48] with the selected FDM machine.

	It classes									
Process	**7**	**8**	**9**	**10**	**11**	**12**	**13**	**14**	**15**	**16**
Casting					x	x	x	x	x	x
Sintering			x	x	x	x				
Milling				x	x	x				
Cutting						x	x	x		
Turning	x	x	x	x						
Drilling						x	x	x		
Injection molding machine		x	x	x	x	x				
FDM (this Study)										
x			x	x	x	x	x			
y			x	x	x	x	x			
z					x	x	x	x		

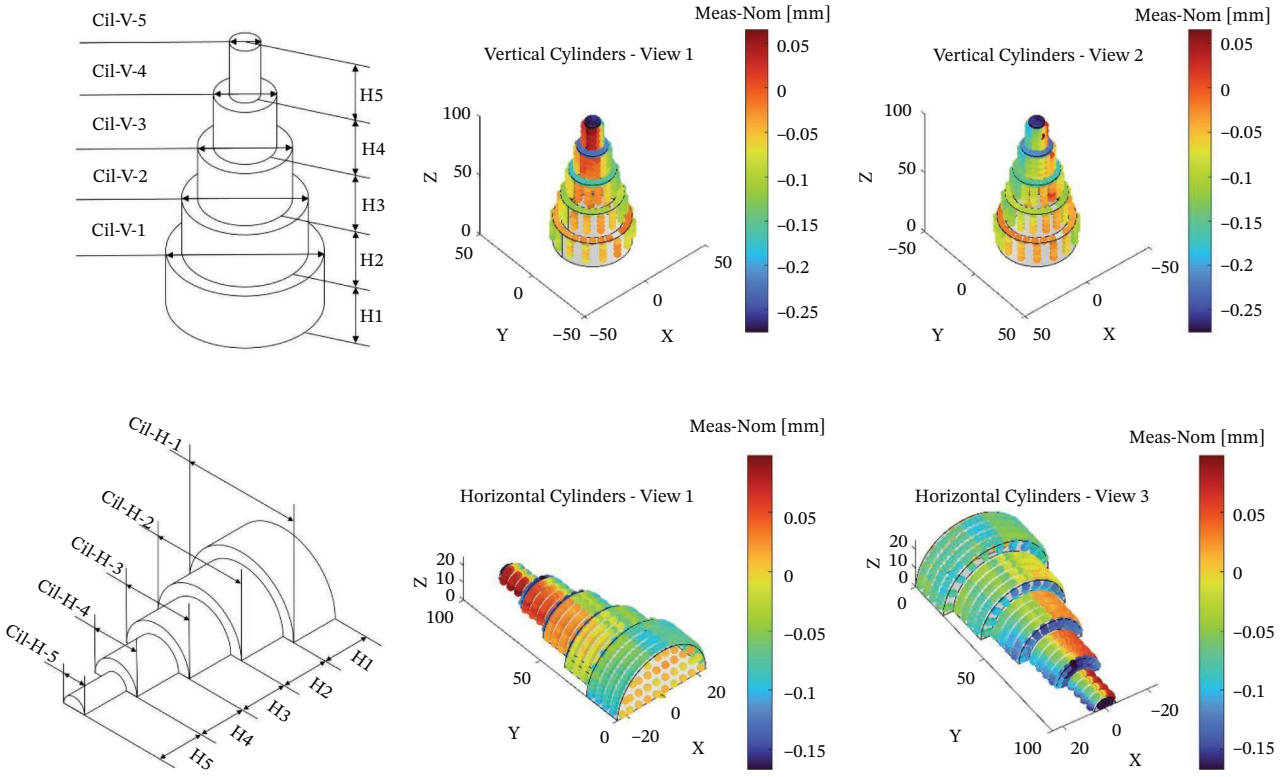

FIGURE 11 | Geometry and dimensional deviation of the vertical (top) and horizontal (bottom) cylinder feature groups. Color maps represent measured-to-nominal deviations in millimeters.

3.2 | GBTA Models

3.2.1 | Vertical and Horizontal Cylinder Profiles

Figure 11 and Table 5 summarize the dimensional and cylindricity deviations for the vertical and horizontal cylinder feature groups. All cylinders exhibit negative diameter deviations, indicating systematic undersizing driven by thermal shrinkage during FDM processing. This contour-driven shrinkage appears approximately constant in magnitude across nominal sizes, so its relative impact becomes more pronounced for smaller features, explaining the apparent increase in percentage error observed at reduced nominal dimensions.

For the horizontal cylinders, the deviations from nominal size were generally larger and exhibited a wider range compared with

TABLE 5 | Dimensional and form errors for vertical and horizontal cylinder features. See also Figures 11 and 12.

Feature	Nominal (mm)	Measured (mm)	Error (%)	Cylindricity (mm)	Feature	Nominal (mm)	Measured (mm)	Error (%)
Cil-V-1	50	49.870	−0.26	0.079	H1	20	19.975	−0.12
Cil-V-2	40	39.861	−0.35	0.076	H2	20	19.923	−0.39
Cil-V-3	30	29.855	−0.48	0.089	H3	20	19.942	−0.29
Cil-V-4	20	19.853	−0.74	0.079	H4	20	19.942	−0.29
Cil-V-5	10	9.892	−1.08	0.052	H5	20	19.953	−0.24
Cil-H-1	50	49.844	−0.31	0.050	H1	20	19.918	−0.41
Cil-H-2	40	39.897	−0.26	0.052	H2	20	19.979	−0.10
Cil-H-3	30	29.894	−0.35	0.054	H3	20	19.974	−0.13
Cil-H-4	20	19.902	−0.49	0.034	H4	20	19.989	−0.05
Cil-H-5	10	9.924	−0.76	0.070	H5	20	19.975	−0.12

the vertical ones. In contrast, the vertical cylinders displayed smaller deviations and a narrower spread between minimum and maximum values. This behavior can be attributed to two distinct mechanisms inherent to the FDM process. As shown by Table 5, diameter deviations for the vertical and horizontal cylinders ranged from −0.108 to −0.149 mm and −0.076 to −0.156 mm, respectively, confirming that part orientation plays an important role in final dimensional accuracy. Two distinct mechanisms govern the orientation-dependent behavior observed. First, the wider deviation range in horizontal cylinders is attributed to the staircase effect, a geometric approximation artifact inherent to layer-by-layer fabrication of curved surfaces. The resulting stepped surface geometry introduces systematic form errors that vary with position along the nominal diameter, increasing the spread between minimum and maximum measured values. Second, the higher mean diameter deviation recorded for vertical cylinders (−0.134 mm) compared with horizontal ones (−0.108 mm) is linked to differences in inter-layer thermal conditions. In vertically oriented parts, the small cross-sectional area per layer reduces the time elapsed between successive deposits at any given point, limiting heat dissipation and promoting localized thermal accumulation. The sustained residual heat induces greater material distortion and reduces dimensional accuracy. In horizontally oriented parts, the larger cross-sectional area increases the effective inter-layer cooling time, allowing more uniform heat dissipation and producing lower mean deviations despite the wider overall range.

These orientation-dependent trends are further reflected in the cylindricity measurements. Vertical cylinders exhibited a mean cylindricity deviation of -0.075 ± 0.014 mm, compared with -0.052 ± 0.013 mm for horizontal cylinders, indicating reduced geometric fidelity in the build direction. Overall, the mean deviation for vertical cylinders (-0.134 ± 0.015 mm) was slightly higher than for horizontal ones (-0.108 ± 0.029 mm), with an absolute mean difference of 0.026 mm. These findings are consistent with the anisotropic cooling and deposition mechanisms characteristic of material extrusion processes, where layer-wise thermal contraction and the staircase effect jointly amplify both dimensional and form inaccuracies in an orientation-dependent manner [46, 49, 50].

Despite this dimensional bias, the low scatter and well-preserved cylindricity values across both orientations indicate process repeatability under the investigated conditions. It should be noted that the reported deviations are specific to the PLA material and printer configuration adopted in this study and may not generalize directly to other FDM setups.

3.2.2 | Curved Profiles

Figure 12 presents the deviation maps for the curved feature groups of the GBTA, with the color scale ranging from −0.25 mm (undersizing) to +0.15 mm (oversizing). The results reveal a systematic negative deviation along the curved vertical walls, indicating global undersizing attributable to thermal shrinkage during cooling. Specifically, the mean deviation along the curved external surfaces was -0.11 ± 0.10 and -0.10 ± 0.10 mm for the 90° 3-curve and 3-curve groups, respectively, with extreme values ranging from −0.28 to +0.10 mm for the former and from −0.26 to +0.15 mm for the latter.

The outer curved surfaces exhibit larger deviations than inner regions, which is attributed to uneven cooling, residual thermal stresses, and geometry-induced shape defects. In material extrusion processes, curved toolpaths promote locally nonuniform heat accumulation and constrained contraction, amplifying dimensional bias along external contours [39, 51]. The increased deviations observed along curved vertical walls therefore highlight the sensitivity of complex geometries to local cooling conditions and path-dependent deposition effects.

Nevertheless, the preservation of overall geometric form and the absence of pronounced distortion indicate that these effects primarily influence absolute dimensional accuracy rather than shape fidelity. In contrast, internal corners and top surfaces display deviations close to the nominal geometry (within approximately 0.15 mm), confirming good local geometric stability under the investigated printing conditions.

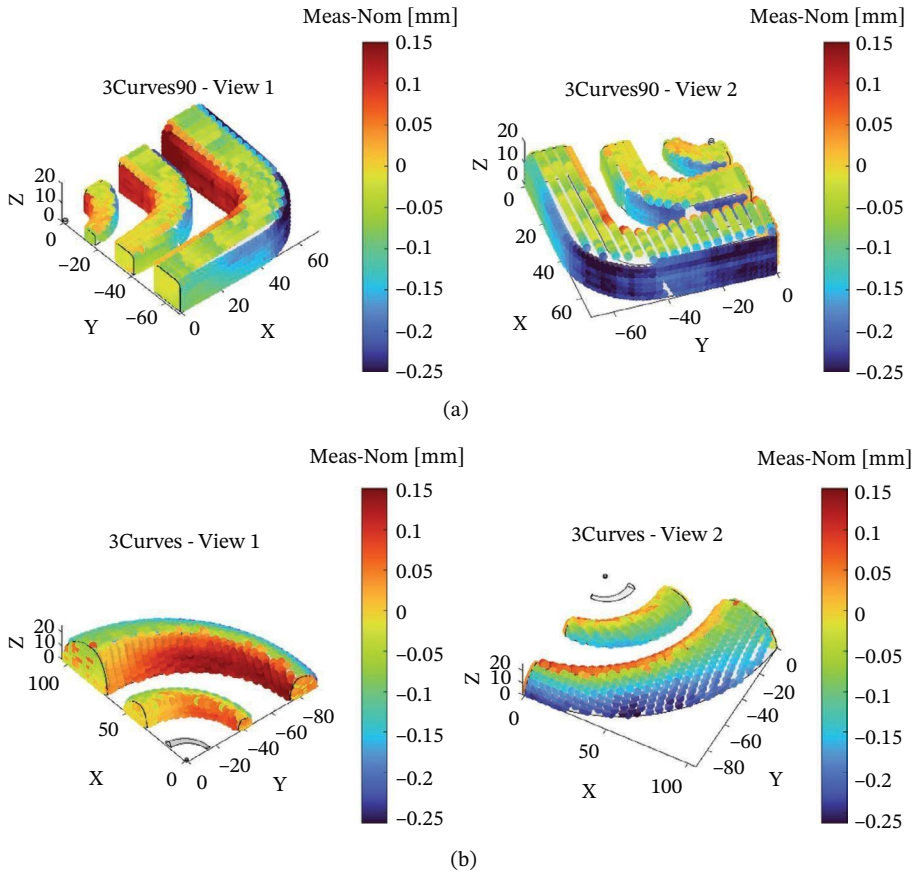

FIGURE 12 | Measured-to-nominal deviation maps for the curved GBTA features: (a) 3-curves 90° feature and (b) 3-curves feature. Color scale ranges from −0.25 (undersizing) to +0.15 mm (oversizing).

Overall, despite the presence of size-dependent shrinkage, the global geometric form is well preserved. The magnitude of the reported deviations is specific to the PLA material and printer configuration adopted in this study, though the qualitative trends are consistent with previously reported thermal contraction behavior in FDM systems [52, 53]. It should also be noted that the adopted GBTA is representative of a door-handle geometry and captures only features relevant to that application. Geometrical features such as internal holes or unsupported overhangs are not explicitly included and would require dedicated benchmark artifacts. Nevertheless, based on findings from prior studies [53, 54], undersizing in internal holes and asymmetric thermal effects in unsupported overhangs would be expected under similar processing conditions.

4 | Conclusion

This study presented a structured methodology for evaluating the dimensional accuracy and process capability of a consumer-level FDM system using staircase samples and a GBTA. Under manufacturer-recommended, nonoptimized printing conditions representative of baseline user-level operation, the investigated Bambu Lab X1-Carbon printer achieved process capability indices $P_{mk} \geq 1.33$ at a 95% confidence level across a wide range of nominal dimensions.

The staircase analysis revealed anisotropic dimensional deviation influenced by build direction, nominal size, spatial location within the build chamber, and fan location. Quantitative spatial comparison confirmed that deviations along the Z direction were statistically dependent on build plate position, consistent with nonuniform cooling effects. Larger nominal features exhibited improved relative precision, whereas smaller dimensions were more sensitive to localized thermal contraction and discretization effects.

GBTA measurements confirmed systematic undersizing of cylindrical and curved geometries. Absolute diameter deviations remained approximately constant across nominal sizes, whereas percentage errors increased for smaller features due to scale effects. Curved vertical walls exhibited larger deviations than internal features, highlighting the influence of contour-driven shrinkage and path-dependent thermal behavior. Despite these dimensional biases, geometric form integrity and repeatability were preserved.

Overall, the results indicate that the investigated FDM system is capable of producing functional polymer components within ISO 286-1 tolerance grades ranging from IT9 to IT14 under baseline operating conditions. These findings are directly applicable to nonstructural interior components fabricated using PLA on similar desktop extrusion systems. Quantitative tolerance values remain machine- and material-specific; however,

the capability-based evaluation framework is transferable to other material extrusion platforms. Specifically, the reported ISO tolerance grades and absolute deviation magnitudes are both material- and system-dependent. The observed trends, instead, such as anisotropic Z-direction behavior, scale-dependent relative error, and spatial variability induced by cooling conditions, are mostly intrinsic to the material extrusion process, although their magnitude may be affected by material properties.

The proposed methodology, combining process capability analysis, standardized tolerance classification, and geometry-representative benchmarking, provides a systematic approach to quantifying dimensional reliability in distributed AM contexts.

Nomenclature

AM	additive manufacturing
CMM	coordinate measuring machine
CNC	computer numerical control
COMPAQT	component for machine performance assessment in quick time
DT	dimensional tolerances
FDM	fused deposition modeling
GBTA	geometric benchmark test artifact
IT	international tolerance
LL	lower limit
M	midpoint
M_i	measurement value
N_i	nominal size
n_i	number of samples
MP	multiple part
MPE	maximum permissible error
PLA	polylactic acid
ppm	parts per million
SP	single part
UL	upper limit
UST	ultimate tensile Strength
$\overline{X}$	mean
σ	standard deviation

Author Contributions

Nikodmose Moges Gebre: writing—original draft, software, methodology, investigation, data curation, conceptualization. Ilaria Cristofolini: writing—review and editing, supervision, methodology, conceptualization. Marco Zago: writing—review and editing, software, methodology, conceptualization. Pasquale Gallo: writing—original draft, review and editing, supervision, methodology, funding acquisition, conceptualization, investigation. Pasquale Gallo and Nikodmose Moges Gebre equally contributed to the work.

Acknowledgments

The authors thank Dr. Daniele Rigotti of the Polymer Lab (Department of Industrial Engineering, University of Trento) for technical assistance and valuable discussions. During the preparation of this work, the authors used ChatGPT (based on GPT-4o, OpenAI) to improve manuscript readability. After using this tool, the authors reviewed and edited the content as needed.

Funding

This study was supported by European Union—Next Generation EU—PNRR, Mission 4 Component 2, Investment 1.3—PE MICS Spoke 5—LOLIMAR Project (PE00000004, CUP D43C22003120001). Open access publishing facilitated by Universita degli Studi di Trento, as part of the Wiley—CRUI-CARE agreement.

Disclosure

The authors take full responsibility for the content of the published article.

Conflicts of Interest

The authors declare no conflicts of interest.

Data Availability Statement

Data are included in the work. Any additional data may be available from the corresponding author upon reasonable request.

References

1. G. A. Pacillo, G. Ranocchiai, F. Loccarini, and M. Fagone, "Additive Manufacturing in Construction: A Review on Technologies, Processes, Materials, and Their Applications of 3d and 4d Printing," *Material Design & Processing Communications* 3, no. 5 (2021): e253, https://doi.org/10.1002/mdp2.253.

2. I.-I. Ailinei, S. V. Galatanu, and L. Marsavina, "The Effects of Layers Orientation on Impact Energy Evaluation of FDM Printed Specimens," *Material Design & Processing Communications* 3, no. 6 (2021): e267, https://doi.org/10.1002/mdp2.267.

3. N. M. Gebre, R. D. Biasi, D. A. Rita, et al., "Towards Standardization of Tensile Testing for Strut-Based Lattices Using Compensated Beam Modeling and Strain-Energy-Based Optimization," *Materials & Design* 258 (2025): 114696, https://doi.org/10.1016/j.matdes.2025.114696.

4. A. Workiye, and Y. Tsega, "Design of Multi-Cell FDM Build Bed Systems for Optimal Material Usage in Additive Manufacturing Process," *Material Design & Processing Communication* 2026, no. 1 (2026): 7334170, https://doi.org/10.1155/mdp2/7334170.

5. S. Singh, S. Ramakrishna, and F. Berto, "3d Printing of Polymer Composites: A Short Review," *Material Design & Processing Communications* 2, no. 2 (2020): e97, https://doi.org/10.1002/mdp2.97.

6. I. Gibson, D. Rosen, and B. Stucker, *Additive Manufacturing Technologies* (Springer, 2015).

7. L. Spitaels, E. N. Fuentes, E. Rivière-Lorphèvre, P.-J. Arrazola, and F. Ducobu, "A Systematic Method for Assessing the Machine Performance of Material Extrusion Printers," *Journal of Manufacturing and Materials Processing* 8, no. 1 (2024): 36, https://doi.org/10.3390/jmmp8010036.

8. A. Weiser, B. Kipp, M. Dillon, et al., "Shrinkage Compensation for FFF Printing for PLA, ABS, and PETG Thermoplastics," in *Proceedings of the Annual General Donald R. Keith Memorial Conference* (2021): 93–98.

9. ASTM, *Terminology for Additive Manufacturing Technologies* (ASTM International, 2012).

10. D. G. Ullman, *The Mechanical Design Process*, 4th ed. (McGraw-Hill, 2010).

11. N. M. Gebre, P. Gallo, and S. Rossi, "Design for Sustainability by Additive Manufacturing: A study of pla-Based Door Handle Redesign," *Sustainability* 17, no. 11 (2025): 4969, https://doi.org/10.3390/su17114969.

12. F. Cerdas, M. Juraschek, S. Thiede, and C. Herrmann, "Life Cycle Assessment of 3d Printed Products in a Distributed Manufacturing System," *Journal of Industrial Ecology* 21, no. S1 (2017): S80–S93, https://doi.org/10.1111/jiec.12618.

13. A. Sapkota, S. K. Ghimire, and S. Adanur, "A Review on Fused Deposition Modeling (FDM)-Based Additive Manufacturing (AM) Methods, Materials and Applications for Flexible Fabric Structures," *Journal of Industrial Textiles* 54 (2024): , https://doi.org/10.1177/15280837241282110.

14. A. du Plessis, G. Schwaderer, I. Cristofolini, M. Zago, and M. Benedetti, "Dimensional Metrology of Additively Manufactured Lattice Structures by Combined Tactile Probe and X-Ray Tomography," *Material Design & Processing Communications* 3, no. 6 (2021): e216, https://doi.org/10.1002/mdp2.216.

15. T. Pereira, J. V. Kennedy, and J. Potgieter, "A Comparison of Traditional Manufacturing vs Additive Manufacturing, the Best Method for the Job," *Procedia Manufacturing* 30 (2019): 11–18, https://doi.org/10.1016/j.promfg.2019.02.003.

16. A. K. Sood, R. Ohdar, and S. Mahapatra, "Improving Dimensional Accuracy of Fused Deposition Modelling Processed Part Using Grey Taguchi Method," *Materials & Design* 30, no. 10 (2009): 4243–4252, https://doi.org/10.1016/j.matdes.2009.04.030.

17. W. C. Lee, C. C. Wei, and S.-C. Chung, "Development of a Hybrid Rapid Prototyping System Using Low-Cost Fused Deposition Modeling and Five-Axis Machining," *Journal of Materials Processing Technology* 214, no. 11 (2014): 2366–2374, https://doi.org/10.1016/j.jmatprotec.2014.05.004.

18. J.-W. Choi, F. Medina, C. Kim, et al., "Development of a Mobile Fused Deposition Modeling System With Enhanced Manufacturing Flexibility," *Journal of Materials Processing Technology* 211, no. 3 (2011): 424–432, https://doi.org/10.1016/j.jmatprotec.2010.10.019.

19. A. Solouki, M. R. Aliha, A. Makui, N. Choupani, and H. Seiti, "Analyzing the Effects of Printing Parameters to Minimize the Dimensional Deviation of Polylactic Acid Parts by Applying Three Different Decision-Making Approaches," *Scientific Reports* 14, no. 1 (2024): 12, https://doi.org/10.1038/s41598-024-78952-9.

20. A. Alafaghani, A. Qattawi, B. Alrawi, and A. Guzman, "Experimental Optimization of Fused Deposition Modelling Processing Parameters: A design-for-Manufacturing Approach," *Procedia Manufacturing* 10 (2017): 791–803, https://doi.org/10.1016/j.promfg.2017.07.079.

21. A. Boschetto, and L. Bottini, "Roughness Prediction in Coupled Operations of Fused Deposition Modeling and Barrel Finishing," *Journal of Materials Processing Technology* 219 (2015): 181–192, https://doi.org/10.1016/j.jmatprotec.2014.12.021.

22. A. Haghighi, and L. Li, "Study of the Relationship Between Dimensional Performance and Manufacturing Cost in Fused Deposition Modeling," *Rapid Prototyping Journal* 24, no. 2 (2018): 395–408, https://doi.org/10.1108/RPJ-11-2016-0177.

23. P. Minetola, M. Galati, F. Calignano, L. Iuliano, G. Rizza, and L. Fontana, "Comparison of Dimensional Tolerance Grades for Metal Am Processes," *Procedia CIRP* 88 (2020): 399–404, https://doi.org/10.1016/j.procir.2020.05.069.

24. L. Spitaels, E. N. Fuentes, V. Dambly, E. Rivière-Lorphèvre, P.-J. Arrazola, and F. Ducobu, "Faster Evaluation of Dimensional Machine Performance in Additive Manufacturing by Using Compaqt Parts," *Journal of Manufacturing and Materials Processing* 8, no. 3 (2024): 100, https://doi.org/10.3390/jmmp8030100.

25. M. Alatefi, A. M. Al-Ahmari, A. Y. AlFaify, and M. Saleh, "A Framework for Fused Deposition Modelling Process Evaluation Using Multivariate Process Capability analysis," *PLoS One* 19, no. 12 (2024): e0308380, https://doi.org/10.1371/journal.pone.0308380.

26. R. Udroiu, and I. C. Braga, "System Performance and Process Capability in Additive Manufacturing: Quality Control for Polymer Jetting," *Polymers* 12, no. 6 (2020): 1292, https://doi.org/10.3390/polym12061292.

27. S. Farah, D. G. Anderson, and R. Langer, "Physical and Mechanical Properties of PLA, and Their Functions in Widespread Applications—A Comprehensive Review," *Advanced Drug Delivery Reviews* 107 (2016): 367–392, https://doi.org/10.1016/j.addr.2016.06.012.

28. J. L. Storck, G. Ehrmann, J. Uthoff, E. Diestelhorst, T. Blachowicz, and A. Ehrmann, "Investigating Inexpensive Polymeric 3d Printed Materials Under Extreme Thermal Conditions," *Materials Futures* 1, no. 1 (2022): 015001, https://doi.org/10.1088/2752-5724/ac4beb.

29. H. Bikas, P. Stavropoulos, and G. Chryssolouris, "Additive Manufacturing Methods and Modelling Approaches: A Critical Review," *The International Journal of Advanced Manufacturing Technology* 83, no. 1-4 (2016): 389–405, https://doi.org/10.1007/s00170-015-7576-2.

30. D. Corapi, G. Morettini, G. Pascoletti, and C. Zitelli, "Characterization of a Polylactic Acid (pla) Produced by Fused Deposition Modeling (FDM) Technology," in *Procedia Structural Integrity* 24 (2019): (Elsevier B.V, 2019), 289–295.

31. I 286-1, "Geometrical Product Specifications (GPS)-Iso Code System for Tolerances on Linear Sizes-Part 1: Basis of Tolerances, Deviations and Fits," (Tech. Rep., ISO, 2010).

32. BI 22514-7:2012, "Standards Publication Statistical Methods in Process Management-Capability and Performance part 7: Capability of Measurement Processes," (Tech. Rep., BSI Standards Limited, 2012).

33. I. Siraj, and P. S. Bharti, "Process Capability Analysis of a 3d Printing Process," *Journal of Interdisciplinary Mathematics* 23, no. 1 (2020): 175–189, https://doi.org/10.1080/09720502.2020.1721711.

34. A. F. Bissell, "How Reliable Is Your Capability Index?," *Journal of the Royal Statistical Society Series C: Applied Statistics* 39, no. 3 (1990): 331–340, https://doi.org/10.2307/2347383.

35. N. Beltrán, B. J. Álvarez, D. Blanco, Á. Noriega, and P. Fernández, "Estimation and Improvement of the Achievable Tolerance Interval in Material Extrusion Additive Manufacturing Through a Multi-State Machine Performance Perspective," *Applied Sciences* 11, no. 12 (2021): 5325, https://doi.org/10.3390/app11125325.

36. RB Group, "Booklet no. 9 Machine and Process Capability," (Tech. Rep., Quality Management in the Bosch Group, 2019).

37. X. Wei, S. Zhang, L. Sun, et al., "Geometric Accuracy and Dimensional Precision in 3d Printing-Based Gear Manufacturing: A study on Interchangeability and Forming Precision," *Polymers* 17, no. 3 (2025): 416, https://doi.org/10.3390/polym17030416.

38. A. Kampker, K. Kreiskother, M. K. Buning, P. Treichel, and J. Theelen, "Automotive Quality Requirements and Process Capability in the Production of Electric Motors," in *Proceedings of the 2017 7th International Electric Drives Production Conference (EDPC)* (IEEE, 2017), 1–8.

39. U. Yaman, "Shrinkage Compensation of Holes via Shrinkage of Interior Structure in FDM Process," *The International Journal of Advanced Manufacturing Technology* 94, no. 5-8 (2018): 2187–2197, https://doi.org/10.1007/s00170-017-1018-2.

40. P. K. Gurrala, and S. P. Regalla, "Multi-Objective Optimisation of Strength and Volumetric Shrinkage of FDM Parts," *Virtual and Physical Prototyping* 9, no. 2 (2014): 127–138, https://doi.org/10.1080/17452759.2014.898851.

41. M. Johar, A. A. Rosli, R. K. Shuib, et al., "Dimensional Stability of Poly (Lactic Acid) (PLA) Parts Fabricated Using Fused Deposition Modelling (FDM)," *Progress in Rubber, Plastics and Recycling Technology* 41, no. 2 (2025): 218–232, https://doi.org/10.1177/14777606241262882.

42. A. A. Al-Tamimi, M. Tlija, M. H. Abidi, A. Anis, and A. E. E. A. Elgawad, "Material Extrusion of Multi-Polymer Structures Utilizing

Design and Shrinkage Behaviors: A Design of Experiment Study," *Polymers* 15, no. 12 (2023): 2683, https://doi.org/10.3390/polym15122683.

43. B. Zharylkassyn, A. Perveen, and D. Talamona, "Effect of Process Parameters and Materials on the Dimensional Accuracy of FDM Parts," *Materials Today: Proceedings* 44 (2021): 1307–1311.

44. O. E. Akbaş, O. Hıra, S. Z. Hervan, S. Samankan, and A. Altınkaynak, "Dimensional Accuracy of FDM-Printed Polymer Parts," *Rapid Prototyping Journal* 26, no. 2 (2019): 288–298, https://doi.org/10.1108/RPJ-04-2019-0115.

45. I. Grgić, M. Karakašić, H. Glavaš, and P. Konjatić, "Accuracy of FDM PLA Polymer 3d Printing Technology Based on Tolerance Fields," *Processes* 11, no. 10 (2023): 2810, https://doi.org/10.3390/pr11102810.

46. L. Spitaels, E. Rivière-Lorphèvre, A. Demarbaix, and F. Ducobu, "Adaptive Benchmarking Design for Additive Manufacturing Processes," *Measurement Science and Technology* 33, no. 6 (2022): 064003, https://doi.org/10.1088/1361-6501/ac5877.

47. A. H. M. Haidiezul, M. H. M. Hazwan, W. S. Lee, N. F. Najihah, and I. Fadhli, "Shrinkage optimisation on the 3d Printed Part Using Full Factorial Design (FFD) Optimisation Approach," *IOP Conference Series: Materials Science and Engineering* 932, no. 1 (2020): 012109, https://doi.org/10.1088/1757-899X/932/1/012109.

48. T. Lieneke, V. Denzer, G. A. Adam, and D. Zimmer, "Dimensional Tolerances for Additive Manufacturing: Experimental Investigation for Fused Deposition Modeling," *Procedia CIRP* 43 (2016): 286–291, https://doi.org/10.1016/j.procir.2016.02.361.

49. T. Koers, and B. Magyar, "Determination and Compensation of the Shrinkage Behavior of Cylindrical Elements in the FDM Process, Proceedings of the Solid Freeform Fabrication 2023," in *34th Annual International Solid Freeform Fabrication Symposium–An Additive Manufacturing Conference Reviewed Paper* (2023): .

50. K. Martusevich, and C. Sen, "An Empirical Design Tool for Estimating in-Plane Diametric Shrinkage and Bulging of Circular Cylinders Made With Fused-Deposition Modeling, Proceedings of the 22nd Design for Manufacturing and the Life Cycle Conference; 11th International Conference on Micro- and Na Nanosystems," in *Volume 4 of International Design Engineering Technical Conferences and Computers and Information in Engineering Conference* (American Society of Mechanical Engineers, 2017).

51. I. Ullah, M. Wasif, and M. Tufail, "Analysis of Shrinkage and Dimensional Accuracy of Additively Manufactured Tooling for the Composite Manufacturing," *International Journal on Interactive Design and Manufacturing* 18, no. 2 (2024): 673–684, https://doi.org/10.1007/s12008-023-01640-x.

52. A. Equbal, R. Murmu, V. Kumar, and M. A. Equbal, "A Recent Review on Advancements in Dimensional Accuracy in Fused Deposition Modeling (FDM) 3d Printing," *AIMS Materials Science* 11, no. 5 (2024): 950–990, https://doi.org/10.3934/matersci.2024046.

53. F. Knoop, and V. Schoeppner, *Geometrical Accuracy of Holes and Cylinders Manufactured With Fused Deposition Modeling* (University of Texas Libraries, 2017).

54. D. Popescu, C. G. Amza, R. Marinescu, M. C. Iacob, and N. L. Căruţaşu, "Investigations on Factors Affecting 3d-Printed Holes Dimensional Accuracy and Repeatability," *Applied Sciences* 13, no. 1 (2023): 41, https://doi.org/10.3390/app13010041.

Appendix A: Detailed Dimensions of the Single Staircase Parts

Figure A1 presented the detailed dimensions of the two single staircase parts used for dimensional tolerance measurements. Geometry 1 (Figure A1-left) has an overall dimension of $18 \times 18 \times 18$ mm, with each step incrementing by 3 mm in all three directions, yielding six nominal measurement steps of 3, 6, 9, 12, 15, and 18 mm. Geometry 2 (Figure A1-right) has an overall dimension of $36 \times 36 \times 36$ mm, with each step incrementing by 6 mm, yielding six nominal measurement steps of 6, 12, 18, 24, 30, and 36 mm.

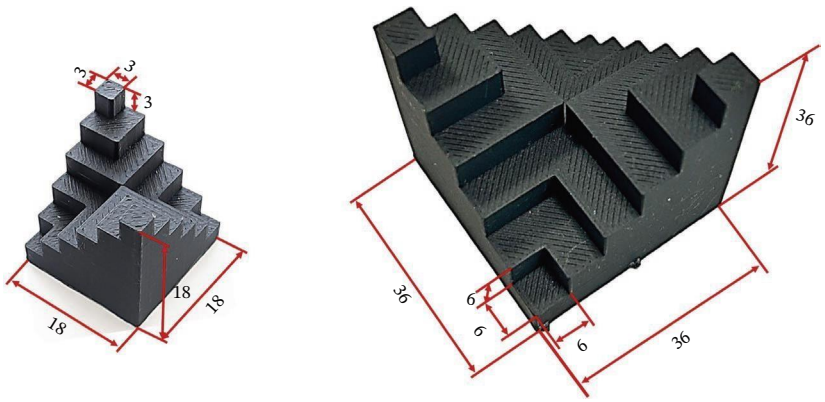

FIGURE A1 | Detailed dimensions of benchmark staircase Geometries 1 (left) and 2 (right) used for dimensional tolerance measurements. Note: All dimensions are in mm.

Appendix B: Standard Tolerance Grades

Nominal size mm		Standard tolerance grades																		
		IT01	IT0	IT1	IT2	IT3	IT4	IT5	IT6	IT7	IT8	IT9	IT10	IT11	IT12	IT13	IT14	IT15	IT16	IT17	IT18
Above	Up to and including	Standard tolerance values																			
		μm													mm						
—	3	0,3	0,5	0,8	1,2	2	3	4	6	10	14	25	40	60	0,1	0,14	0,25	0,4	0,6	1	1,4
3	6	0,4	0,6	1	1,5	2,5	4	5	8	12	18	30	48	75	0,12	0,18	0,3	0,48	0,75	1,2	1,8
6	10	0,4	0,6	1	1,5	2,5	4	6	9	15	22	36	58	90	0,15	0,22	0,36	0,58	0,9	1,5	2,2
10	18	0,5	0,8	1,2	2	3	5	8	11	18	27	43	70	110	0,18	0,27	0,43	0,7	1,1	1,8	2,7
18	30	0,6	1	1,5	2,5	4	6	9	13	21	33	52	84	130	0,21	0,33	0,52	0,84	1,3	2,1	3,3
30	50	0,6	1	1,5	2,5	4	7	11	16	25	39	62	100	160	0,25	0,39	0,62	1	1,6	2,5	3,9
50	80	0,8	1,2	2	3	5	8	13	19	30	46	74	120	190	0,3	0,46	0,74	1,2	1,9	3	4,6
80	120	1	1,5	2,5	4	6	10	15	22	35	54	87	140	220	0,35	0,54	0,87	1,4	2,2	3,5	5,4
120	180	1,2	2	3,5	5	8	12	18	25	40	63	100	160	250	0,4	0,63	1	1,6	2,5	4	6,3
180	250	2	3	4,5	7	10	14	20	29	46	72	115	185	290	0,46	0,72	1,15	1,85	2,9	4,6	7,2
250	315	2,5	4	6	8	12	16	23	32	52	81	130	210	320	0,52	0,81	1,3	2,1	3,2	5,2	8,1

FIGURE A2 | Standard tolerance grades for nominal sizes up to 250 mm according to ISO 286-1.

Appendix C: *t*-Test Analysis

A two-sample *t*-test was conducted to assess the influence of build plate location by comparing dimensional deviations between regions adjacent to the cooling fan and those on the opposite side, as shown in Figure A3. Each region comprised several measurement locations, and each location included multiple dimensional measurements. To ensure statistical independence, the analysis was performed using mean deviation values computed for each location. This provided a statistical basis for evaluating whether localized cooling conditions produced systematic differences in final part dimensions. Main steps and equations are listed from Equation (C.1)–(C.5).

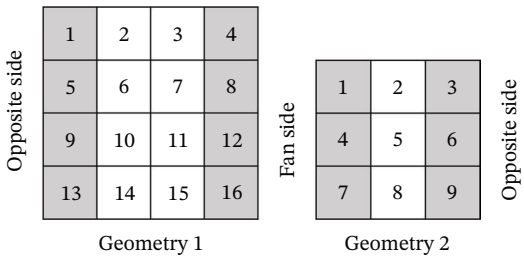

FIGURE A3 | Selection of measurement locations used in the *t*-test analysis for fan-side and opposite-side regions in Geometry 1 (left) and Geometry 2 (right). Each location includes multiple dimensional measurements, from which a representative mean deviation is computed. These location-level mean values are used as independent observations in the statistical comparison between regions.

1. Deviation calculation: The deviation D_i between the nominal size N_i and the measured value M_i was calculated for each individual measurement as:

$$D_i = M_i - N_i \tag{C.1}$$

The build plate was partitioned into two distinct regions based on lateral grid coordinates: (1) fan-side, corresponding to measurement locations {4,8,12,16} or {1,4,7}, adjacent to the cooling fan; and (2) opposite-side, corresponding to measurement locations {1,5,9,13} or {3,6,9}, located furthest from the cooling source.

2. Arithmetic mean ($\overline{D}_{loc}$) and sample standard deviation (s) calculation:

a. Location-level mean deviation: For each measurement location, a representative mean deviation was computed from the corresponding set of individual measurement deviations:

$$\overline{D}_{loc} = \frac{1}{n_m}\sum_{i=1}^{n_m} D_i \tag{C.2}$$

where n_m is the number of individual measurements at a given location.

b. Region-level statistics: The location-level mean deviations were then grouped into fan-side and opposite-side regions. For each region, the mean and standard deviation were computed as follows:

$$\overline{D}_{region} = \frac{1}{n_l}\sum_{j=1}^{n_l} \overline{D}_{loc,j} \tag{C.3}$$

$$s = \sqrt{\frac{\sum_{j=1}^{n_l}\left(\overline{D}_{loc,j} - \overline{D}_{region}\right)^2}{n_l - 1}} \tag{C.4}$$

where n_l is the number of independent measurement locations in each region.

3. Two-Sample *t*-test (t): An independent two-sample *t*-test was employed to determine whether the mean deviations of the fan-side ($\overline{D}_f$) and opposite-side ($\overline{D}_o$) regions were statistically different. The test was performed using location-level mean deviations as independent observations.

The t-statistic is defined as follows:

$$(C.5)\quad t = \frac{\overline{D}_f - \overline{D}_o}{\sqrt{\left(\left(s_f^2/n_f\right) + \left(s_o^2/n_o\right)\right)}}$$

where s_f and s_o represent the standard deviations of the location-level mean deviations for the fan-side and opposite-side regions, respectively, and n_f and n_o denote the number of independent measurement locations in each region.

4. p Value and Significance: The p value enables quantitative comparison of location dependent deviations. Specifically, if $p < 0.05$ for the test axis, the results indicate a statistically significant difference in mean deviations between the fan-side and opposite-side regions, suggesting that spatial location influences dimensional accuracy.

Appendix D: Heat Map Representation of Average Relative Deviations

For the two staircase geometries (Geometry 1 and Geometry 2), the average relative deviations (mm) are presented as heat maps in Figures A4 and A5. For Geometry 1 (Figure A4), the deviations are predominantly negative, indicating that printed parts tend to be slightly undersized. The largest deviations occur along the Z-axis, particularly on the right side of the build plate, likely due to uneven cooling induced by the fan, which leads to

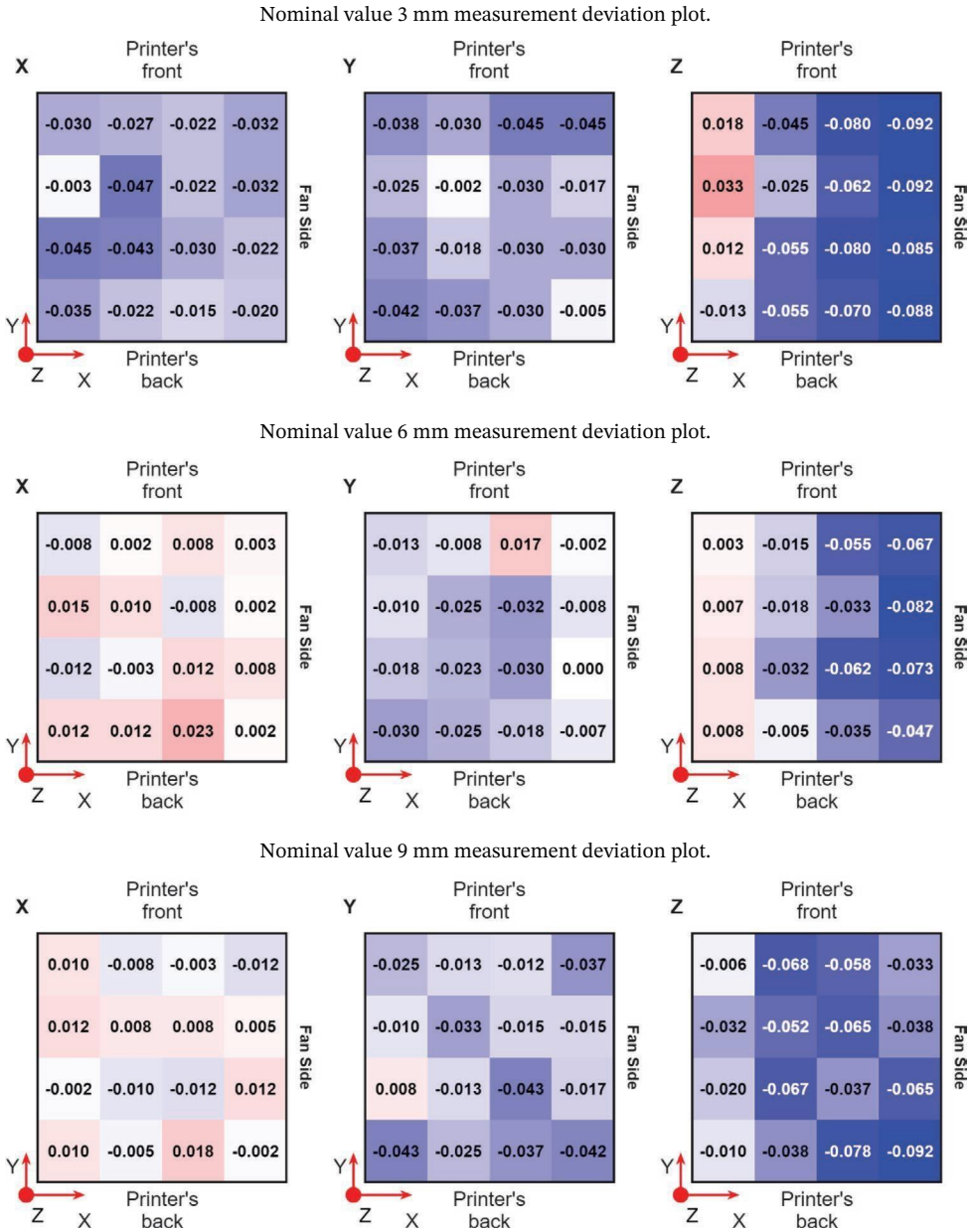

FIGURE A4 | Heat maps of average relative deviations (mm) for Geometry 1 staircase parts at nominal dimensions from 3 to 18 mm. Each square represents a measurement location within the build chamber. Blue indicates negative deviations (shrinkage), whereas red indicates positive deviations (expansion).

thermal gradients and localized stress. In contrast, positive deviations are observed on the left side and along the x-axis for smaller nominal sizes (6 and 9 mm), suggesting localized expansion associated with build plate adhesion effects.

For Geometry 2 (Figure A5), a clear scale-dependent behavior is observed: larger parts exhibit negative deviations (shrinkage), whereas smaller parts show positive deviations (expansion). This is reflected in the predominantly blue regions for larger nominal sizes and red regions for smaller ones. Larger deviations are also noted at the rear of the build plate, where direct contact enhances shrinkage, whereas elevated, smaller features tend to expand due to different thermal conditions during cooling and solidification.

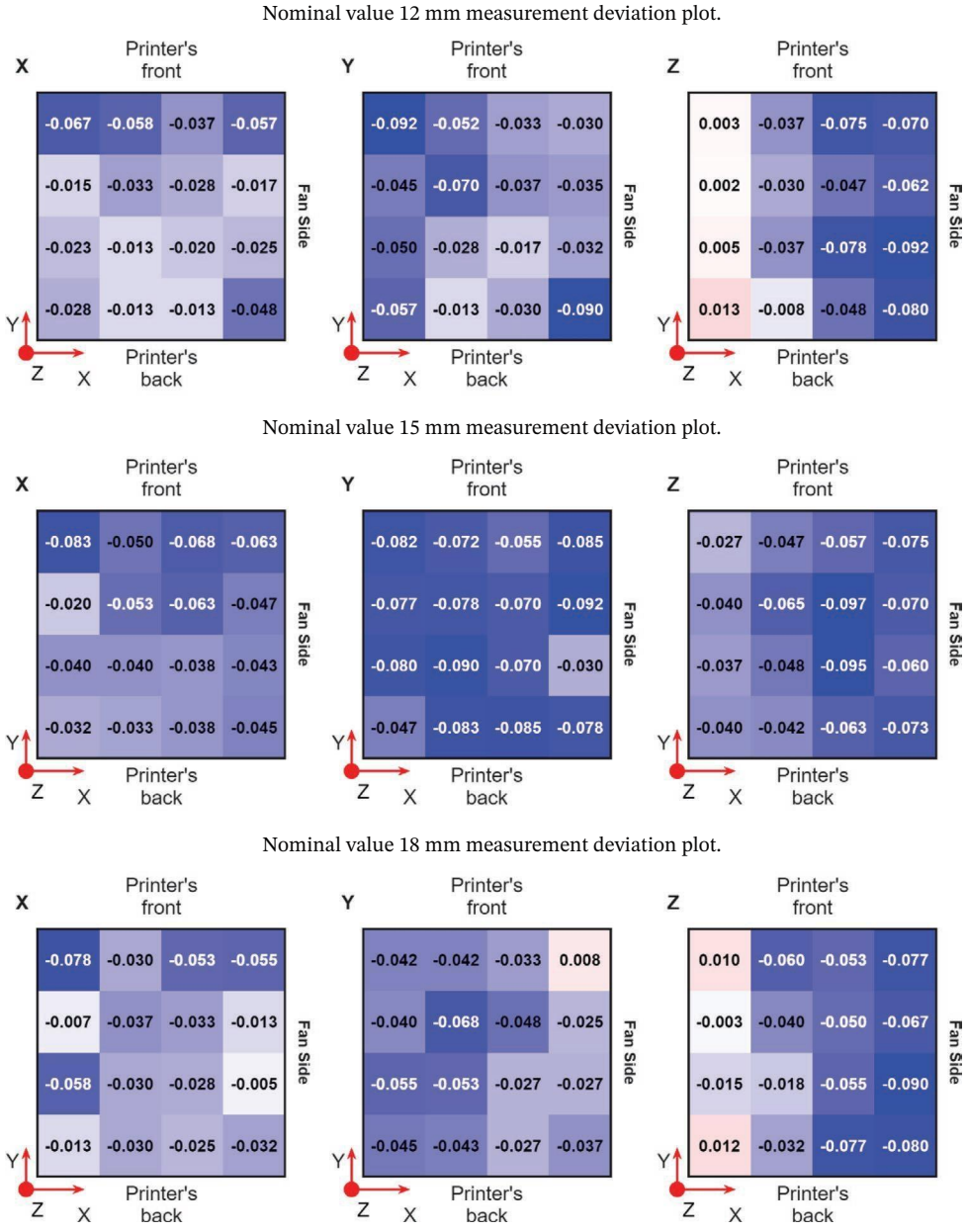

FIGURE A4 | **(CONTINUED)**

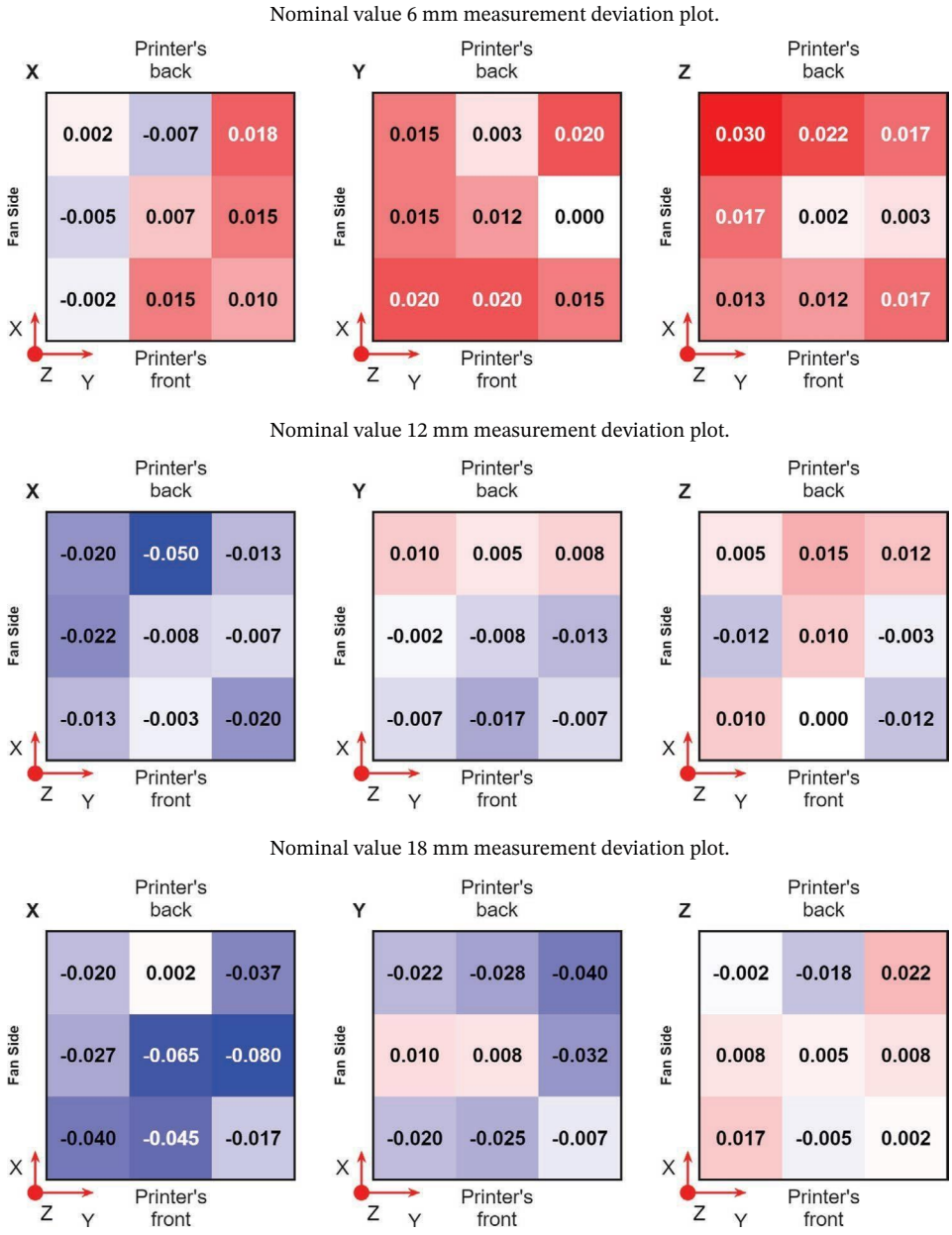

FIGURE A5 | Heat maps of average relative deviations (mm) for Geometry 2 staircase parts at nominal dimensions from 6 to 36 mm. Each square represents a measurement location within the build chamber. Blue indicates negative deviations (shrinkage), whereas red indicates positive deviations (expansion).

Nominal value 24 mm measurement deviation plot.

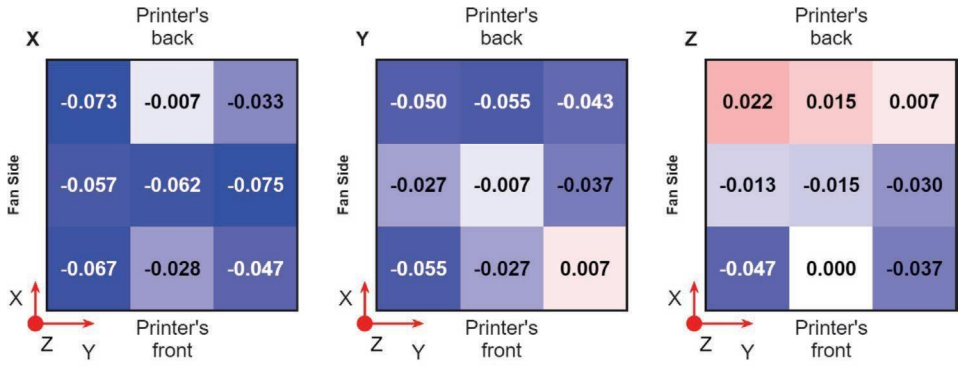

Nominal value 30 mm measurement deviation plot.

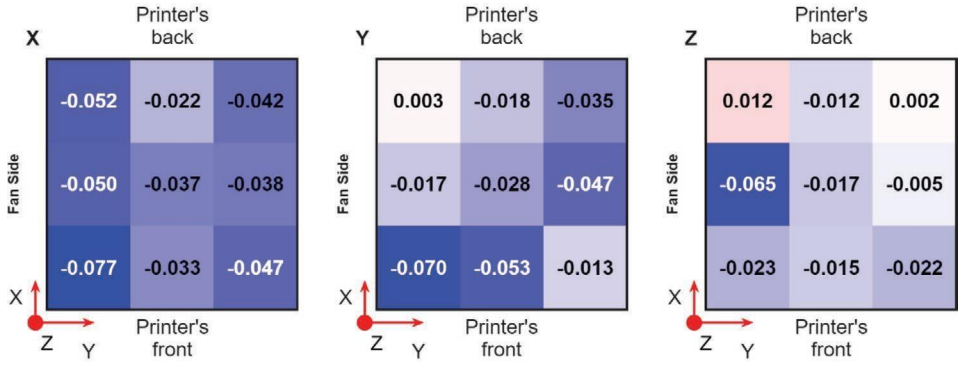

Nominal value 36 mm measurement deviation plot.

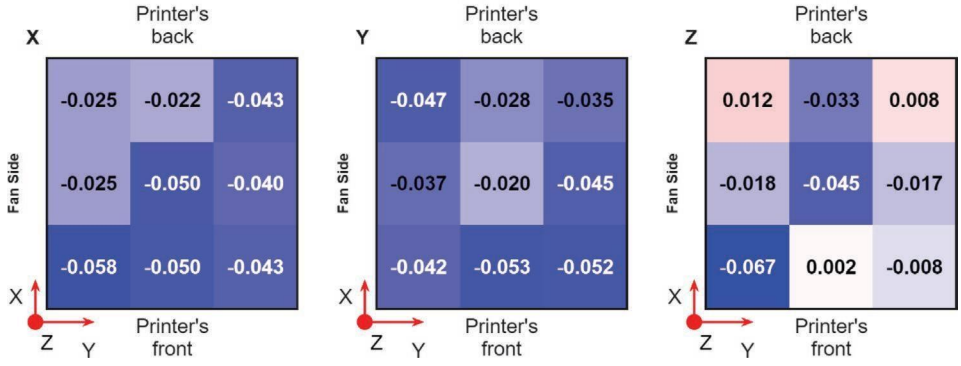

FIGURE A5 | (CONTINUED)